The role of lateral erosion in the evolution of nondendritic drainage networks to dendricity and the persistence of dynamic networks

Jeffrey S. Kwang[a,b,1], Abigail L. Langston[c], and Gary Parker[b,d,1]

[a]Department of Geosciences, University of Massachusetts Amherst, Amherst, MA 01003; [b]Department of Civil and Environmental Engineering, University of Illinois Urbana–Champaign, Urbana, IL 61801; [c]Department of Geography and Geospatial Sciences, Kansas State University, Manhattan, KS 66506; and [d]Department of Geology, University of Illinois Urbana–Champaign, Urbana, IL 61801

Contributed by Gary Parker, March 8, 2021 (sent for review July 28, 2020; reviewed by Katherine R. Barnhart, William E. Dietrich, and Scott McCoy)

Dendritic, i.e., tree-like, river networks are ubiquitous features on Earth's landscapes; however, how and why river networks organize themselves into this form are incompletely understood. A branching pattern has been argued to be an optimal state. Therefore, we should expect models of river evolution to drastically reorganize (suboptimal) purely nondendritic networks into (more optimal) dendritic networks. To date, current physically based models of river basin evolution are incapable of achieving this result without substantial allogenic forcing. Here, we present a model that does indeed accomplish massive drainage reorganization. The key feature in our model is basin-wide lateral incision of bedrock channels. The addition of this submodel allows for channels to laterally migrate, which generates river capture events and drainage migration. An important factor in the model that dictates the rate and frequency of drainage network reorganization is the ratio of two parameters, the lateral and vertical rock erodibility constants. In addition, our model is unique from others because its simulations approach a dynamic steady state. At a dynamic steady state, drainage networks persistently reorganize instead of approaching a stable configuration. Our model results suggest that lateral bedrock incision processes can drive major drainage reorganization and explain apparent long-lived transience in landscapes on Earth.

drainage networks | landscape evolution | lateral migration | drainage reorganization

What should a drainage network look like? Fig. 1*A* shows a single channel, winding its way through the catchment so as to have access to water and sediment from unchannelized zones in the same manner as the dendritic (tree-like) network of Fig. 1*B*. It appears straightforward that the dendritic pattern is a model for nature, and the single channel is not. Dendritic drainage networks are called such because of their similarity to branching trees, and their patterns are "characterized by irregular branching in all directions" (1) with "tributaries joining at acute angles" (2). Drainage networks can also take on other forms such as parallel, pinnate, rectangular, and trellis in nature (2). However, drainage networks in their most basic form without topographic, lithologic, and tectonic constraints should tend toward a dendritic form (2). In addition, drainage networks that take a branching, tree-like form have been argued to be "optimal channel networks" that minimize total energy dissipation (3, 4). Therefore, we would expect that models simulating river network formation, named landscape evolution models (LEMs), that use the nondendritic pattern of Fig. 1*A* as an initial condition to massively reorganize and approach the dendritic steady state of Fig. 1*B*. To date, no numerical LEM has shown the ability to do this. Here, we present a LEM that can indeed accomplish such a reorganization. A corollary of this ability is the result that landscapes approach a dynamic, rather than static steady state.

There is indeed debate as to whether landscapes tend toward an equilibrium that is frozen or highly dynamic (5). Hack (6) hypothesized that erosional landscapes attain a steady state where "all elements of the topography are downwasting at the same rate." This hypothesis has been tested in numerical models and small-scale experiments. Researchers found that numerical LEMs create static topographies (7, 8). In this state, erosion and uplift are in balance in all locations in the landscape, resulting in landscapes that are dissected by stable drainage networks in geometric equilibrium (9). The landscape has achieved geometric equilibrium in planform when a proxy for steady-state river elevation, named χ (10), has equal values across all drainage divides. In contrast, experimental landscapes (7, 11) develop drainage networks that persistently reorganize. Recent research on field landscapes suggests that drainage divides migrate until reaching geometric equilibrium (9), but other field-based research suggests that landscapes may never attain geometric equilibrium (12).

The dynamism of the equilibrium state determines the persistence of initial conditions in experimental and model landscapes. It is important to understand initial condition effects (13) to better constrain uncertainty in LEM predictions. Kwang and Parker (7) demonstrate that numerical LEMs exhibit "extreme memory," where small topographic perturbations in initial conditions are amplified and preserved during a landscape's evolution (Fig. 2*A*). Extreme memory in the numerical models is closely related to the feasible optimality phenomenon found within the research on optimal channel networks (4). These researchers suggest that nature's search for the most "stable" river network configuration is "myopic" and unable to find configurations that completely ignore their initial condition. In contrast to numerical models, experimental landscapes (7, 11) reach a highly dynamic state where all

Significance

Most of Earth's landscapes are dissected by rivers, which are important for providing water, food, and energy resources. From remote imaging, we see that rivers organize themselves into dendritic (tree-like) networks. The shape and organization of river networks determine how and where water and sediment are routed on Earth. To date, models of river network formation, named landscape evolution models, are unable to explain how nondendritic networks evolve into strongly branching systems. Here, we capture this evolution utilizing a model that incorporates how rivers erode in the lateral direction.

Author contributions: J.S.K., A.L.L., and G.P. designed research; J.S.K. and A.L.L. performed research; J.S.K. and A.L.L. analyzed data; and J.S.K. and A.L.L. wrote the paper.

Reviewers: K.R.B., US Geological Survey; W.E.D., University of California, Berkeley; and S.M., University of Nevada, Reno.

The authors declare no competing interest.

[1]To whom correspondence may be addressed. Email: jeffskwang@gmail.com or parkerg@illinois.edu.

This article contains supporting information online at https://www.pnas.org/lookup/suppl/doi:10.1073/pnas.2015770118/-/DCSupplemental.

Published April 12, 2021.

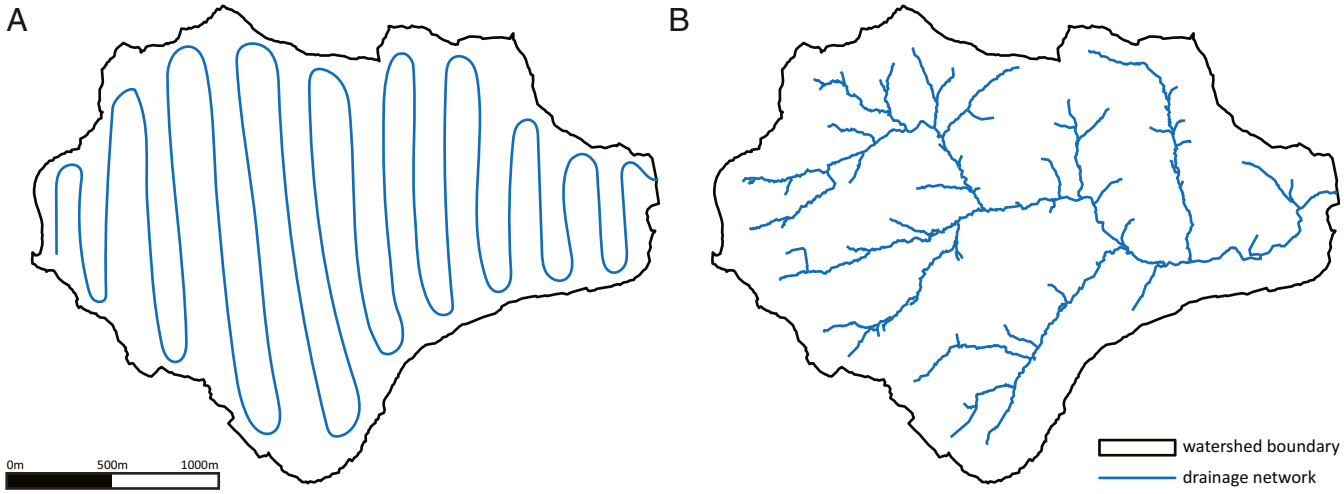

Fig. 1. Schematic diagram of a nondendritic and a dendritic drainage network. This figure shows the Wolman Run Basin in Baltimore County, MD (*A*) drained by a single channel winding across the topography and (*B*) drained by a dendritic network of channels. Both networks have similar drainage densities (53, 54), but there is a stark difference between their stream ordering (53–56). This figure invites discussion as to how a drainage system might evolve from the configuration of *A* to that of *B*.

traces of initial surface conditions are erased by drainage network reorganization. It has been hypothesized that lateral erosion processes are responsible for drainage network reorganization in landscapes (7, 14); these processes are not included in most LEMs.

Most widely used LEMs simulate incision into bedrock solely in the vertical direction. However, there is growing recognition that bedrock channels also shape the landscape by incising laterally (15, 16). Lateral migration into bedrock is important for the creation of strath terraces (17, 18) and the morphology of wide bedrock valleys (19–21). Recently, Langston and Tucker (22) developed a formulation for lateral bedrock erosion in LEMs. Here, we implement their submodel to explore the long-term behavior of LEMs that incorporate lateral erosion.

The LEM submodel of Langston and Tucker (22) allows for channels to migrate laterally. By including this autogenic mechanism, we hypothesize that lateral bedrock erosion creates instabilities that 1) shred (23) the memory of initial conditions such as the unrealistic configurations of Fig. 1*A* and 2) produce landscapes that achieve a statistical steady state instead of a static one. By incorporating the lateral incision component (22) into a LEM, we aim to answer the following: 1) What controls the rate of decay of signals from initial conditions? 2) What are the frequency and magnitude of drainage reorganization in an equilibrium landscape? 3) What roles do model boundary conditions play in landscape reorganization?

Steady-State Background

Willett and Brandon (24) described two types of steady states. The simplest case, a flux steady state, requires the sum of erosional fluxes across the landscape to equal the total amount of flux entering the landscape (via uplift or baselevel lowering). The second case, a more stringent definition, is "static steady state" [also named topographic steady state in Willett and Brandon (24)]. Here, local erosion rates across the entire landscape are equal to an uplift or base level lowering rate, resulting in a frozen landscape with a static drainage network, which also satisfies the flux steady-state condition.

We present a modified definition named "dynamic steady state," where a landscape achieves a flux steady state but not a static steady state. Under this condition, the total amount of flux entering and leaving the landscape is balanced, but a precise local balance between uplift and erosion at all locations in the catchment will never occur. Generally, experimental landscapes (7, 11) tend toward dynamic steady states, whereas numerical LEMs (7, 8) achieve static steady states with frozen drainage networks. We emphasize that both dynamic steady state and static steady state would satisfy the broad definition of Hack's "dynamic equilibrium," where "all elements of the topography are downwasting at the same rate" (6).

There have been attempts to create LEMs that attain a dynamic steady state. LEMs with modified flow routing schemes (25) have been shown to create persistent local drainage migration, i.e., a dynamic steady state, but this modification is likely to "underestimate the extent of lateral drainage migration in nature" (25). Conversely, Perron et al. (26) reached the opposite conclusion, where LEMs with a similar flow routing algorithm did attain a static steady state, and instead suggest that the unsteadiness in previous models (25) occurred due to a landsliding submodel (27).

Some experimental landscapes (28–31) were significantly less dynamic (i.e., tending toward static steady state) than other experiments (7, 11, 32–34). Paola et al. (35) hypothesized that the relevant difference was experimental geometry. The static steady-state experiments (28–31) featured open boundaries along all landscape's edges that allowed material to exit, whereas the dynamic steady-state experiments (7, 11, 32–34) constrained the locations where material could exit. In general, closed boundary conditions (7, 11) created large complex drainage basins that were dynamic, while open boundaries (28–31) promoted many relatively small subbasins that were generally static.

Results

We use a landscape evolution model incorporating lateral erosion (LEM-wLE) to 1) determine which steady-state behavior landscapes approach, 2) test whether initial topographies are preserved or shredded, and 3) determine what sets the persistence of initial conditions. In Fig. 2, we compare the results of a standard landscape evolution model without a lateral erosion component (LEM-woLE) to LEM-wLE (see *Materials and Methods*). The ratio of lateral and vertical rock erodibility (K_L/K_v) is set to 1 (22). As with Hasbargen and Paola (11), we use a temporal scale that refers to the time it takes for the landscape to erode through one unit of relief, i.e., the maximum elevation difference in the landscape. For our parameter set, the relief is ~200 m, and the uplift rate is set to 1 mm/y. Therefore, the time it takes for one unit of relief (RU) to be eroded is ~200 ky.

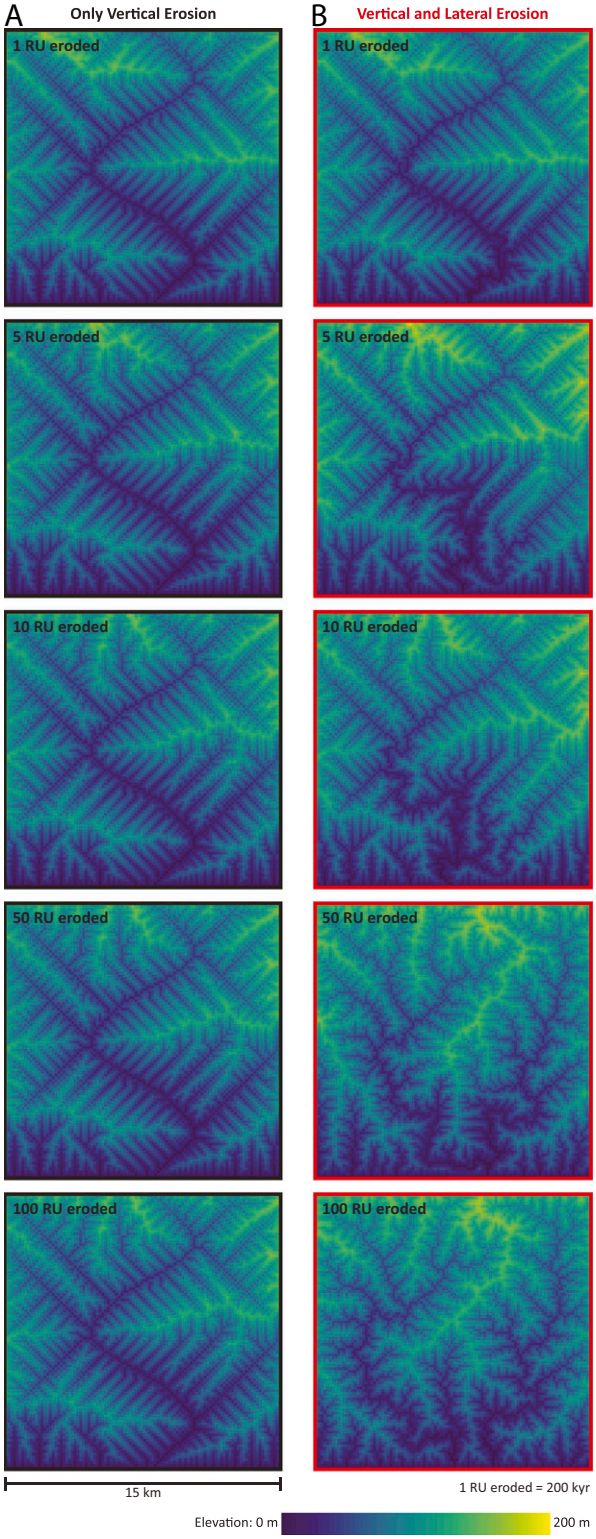

Fig. 2. A comparison of LEM-woLE (*A*) and LEM-wLE (*B*). Both models utilize the same initial condition, i.e., an initially flat topography with an embedded sinusoidal channel (1.27 m deep) without added topographic perturbations. Without perturbations, the landscape produces angular tributaries that are attached to the main sinusoidal channel (compare with *SI Appendix*, Fig. S7). Here, LEM-wLE quickly shreds the signal of the initial condition over time, removing the angular tributaries. By 10 RUs eroded the sinusoidal signal is mostly erased. After 100 RUs, the drainage network continues to reorganize itself (i.e., dynamic steady state). The landscape continues to reorganize as shown in Movies S1.

Fig. 2 shows the evolution of surface topography using LEM-woLE (Fig. 2*A*) and LEM-wLE (Fig. 2*B*), utilizing a flat landscape with an embedded planform sinusoidal channel as the initial topography. For both simulations, the landscapes reach flux steady states after eroding through ~1 RU (*SI Appendix*, Fig. S1). Using LEM-woLE (Fig. 2*A*), the landscape achieves static steady state after eroding through ~2 RUs. We note that Howard (36) estimates erosion into ~3 RUs is required to reach equilibrium in LEMs. In this state, the drainage network stabilizes, reaching geometric equilibrium. The drainage network prominently features a sinusoidal channel inherited from the initial condition with many parallel nonbranching tributaries. At equilibrium, slope and drainage area follow a tight power law relationship (*SI Appendix*, Fig. S2). In contrast, landscapes simulated using LEM-wLE (Fig. 2*B*) feature a drainage network that reorganizes and shreds the nondendritic initial condition signal over time. After eroding through 50 to 100 RUs, the sinusoidal signal is completely erased and is substituted by a dendritic drainage network, where the nonbranching tributaries are converted into dendritic ones. The landscape continues to persistently reorganize its drainage networks (Movies S1–S2). Slope and drainage area also follow a power law relationship; however, there is significant scatter (*SI Appendix*, Fig. S2).

We also test other initial conditions that create drainage networks found in nature (*SI Appendix*, Figs. S3–S6 and Movies S4–S12), as well an initial topography with a sinusoidal channel with added topographic perturbations (*SI Appendix*, Fig. S7 and Movies S13–S15). Each initial condition creates drastically different steady-state landscapes using LEM-woLE (*SI Appendix*, Fig. S3). In contrast, LEM-wLE erases the initial conditions and tends toward a dynamic steady state.

The degree of memory of the initial condition is quantified with a correlation coefficient, C:

$$C = \frac{\sum_{i=1}^{M}\sum_{j=1}^{N}\left[\left(\eta_{i,j}-\overline{\eta}\right)\left(\eta_{ref,i,j}-\overline{\eta_{ref}}\right)\right]}{\sqrt{\sum_{i=1}^{M}\sum_{j=1}^{N}\left(\eta_{i,j}-\overline{\eta}\right)^2}\sqrt{\sum_{i=1}^{M}\sum_{j=1}^{N}\left(\eta_{ref,i,j}-\overline{\eta_{ref}}\right)^2}}, \quad [1]$$

where MN is the number of cells in the domain, i and j are cell indices, and η is elevation. This equation calculates how a landscape's elevation field (η) is correlated to the elevation field of a reference topography (η_{ref}), which is the static steady-state topography produced by LEM-woLE. Using C, we compare the dynamic steady-state topographies in LEM-wLE to the static steady-state topography from LEM-woLE (Fig. 3*A*). Higher values of correlation signify that the topographies are alike and that memory of the initial condition is retained. At the beginning of the LEM-woLE simulation (black dashed-line), correlation increases until it evolves toward the reference topography (Fig. 3*A*). After attaining static steady state, all subsequent landscapes are perfectly correlated ($C = 1$) to the reference topography. In the LEM-wLE simulation (red line), C decreases during evolution, indicating the shredding of the initial condition signal (Fig. 3*A*). The landscapes still retain some correlation because all the landscapes have a downslope trend toward the outlet.

After the initial condition signal is erased, the landscape in the LEM-wLE model continues to persistently reorganize. The drainage networks in the LEM-wLE never become static and are in constant geometric disequilibrium. The degree of dynamism in LEM-wLE is quantified by the wiggle number, Wi, here defined as follows:

$$Wi = \frac{1}{UMN}\sum_{i=1}^{M}\sum_{j=1}^{N}\left|U - E_{i,j}\right|, \quad [2]$$

where U is uplift, and E is the total incision. Wi represents the spatial variability in erosion rates, so that higher values correspond to more dramatic and frequent drainage network reorganization.

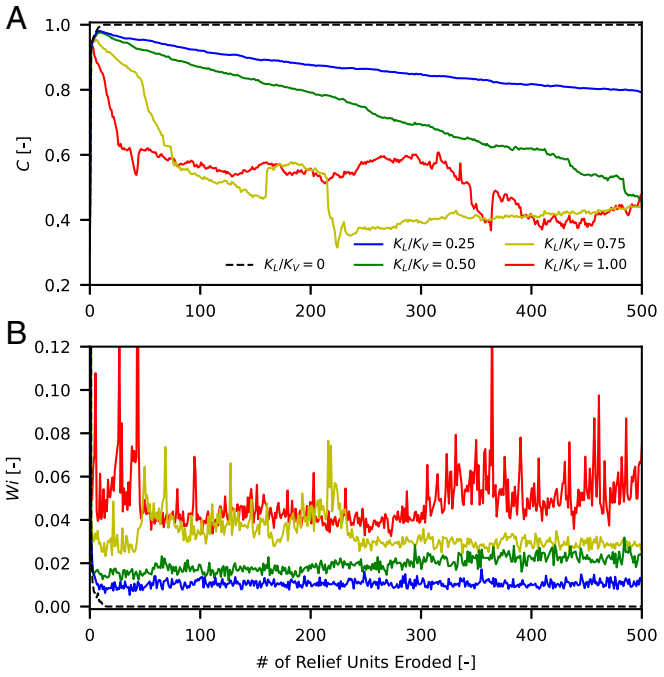

Fig. 3. Time series of the correlation coefficient (*A*) and wiggle number (*B*) over 500 units of relief eroded. A decrease in correlation coefficient represents the removal of the initial condition signal. Here, LEM-woLE (black dashed line) shows extreme memory, while LEM-wLE (colored lines) tends to shred the signal of the initial condition over time. Correlation coefficient decreases at a faster rate as K_L/K_V increases. Correlation does not tend toward zero because all landscapes maintain a general downslope trend toward the outlet. The wiggle number represents the degree of dynamism in landscape, which increases with the ratio of K_L/K_V.

When *Wi* is zero, the landscape has achieved a static steady state and the drainage network is frozen. Nonzero values of *Wi* indicate a dynamic steady state, with larger values corresponding to stronger deviation from a static state. In LEM-woLE (black dashed line), *Wi* reaches zero after attaining static steady state, but *Wi* in LEM-wLE (red line) remains positive, indicating a dynamic steady state (Fig. 3*B*). *C* and *Wi* are also analyzed for additional initial conditions (*SI Appendix*, Fig. S8).

The main control on the behavior of LEM-wLE is the ratio of lateral and vertical rock erodibility, K_L/K_V. We ran additional simulations (*SI Appendix*, Fig. S9 and Movies S16–S24) where K_L/K_V ranges from 0.25 to 1.0, which are summarized in Fig. 3. Fig. 3*A* shows that the reduction in the ratio K_L/K_V decelerates the decay rate of *C*. In other words, the initial condition memory persists over longer periods when K_L/K_V is low. Fig. 3*B* depicts a systematic increase in *Wi* as K_L/K_V increases, meaning, the frequency of drainage reorganization and the level of dynamism increase with K_L/K_V. Furthermore, these results demonstrate a continuum behavior between LEM-wLE and LEM-woLE, which is LEM-wLE utilizing a ratio of zero.

Last, we explored how boundary conditions affect the levels of dynamism of steady-state landscapes in LEM-wLE ($K_L/K_V = 1.0$) (Movies S25–S33). Fig. 4 depicts a time series of *Wi* for three different boundary condition configurations, while keeping the domain size constant. We use open boundaries that allow sediment and water to exit and closed boundaries that do not. Closing the domain's boundaries constrains the outlet locations of catchment, creating a landscape dissected by relatively few but large subbasins. Fig. 4 shows that more open configurations have significantly lower values of *Wi*. Therefore, closed boundaries promote higher levels of dynamism, consistent with the hypothesis of Paola et al. (35).

Discussion

The behavior of LEM-wLE significantly differs from LEM-woLE. LEMs that ignore lateral erosion exhibit extreme memory of initial conditions (7), but LEM-wLE shreds signals of the initial condition. In addition, landscapes in LEM-wLE achieve a dynamic steady state where channel migration causes dramatic persistent drainage network reorganization and geometric disequilibrium, even while under the assumptions of homogenous materials and a steady, unform uplift forcing. In contrast, LEM-woLE requires

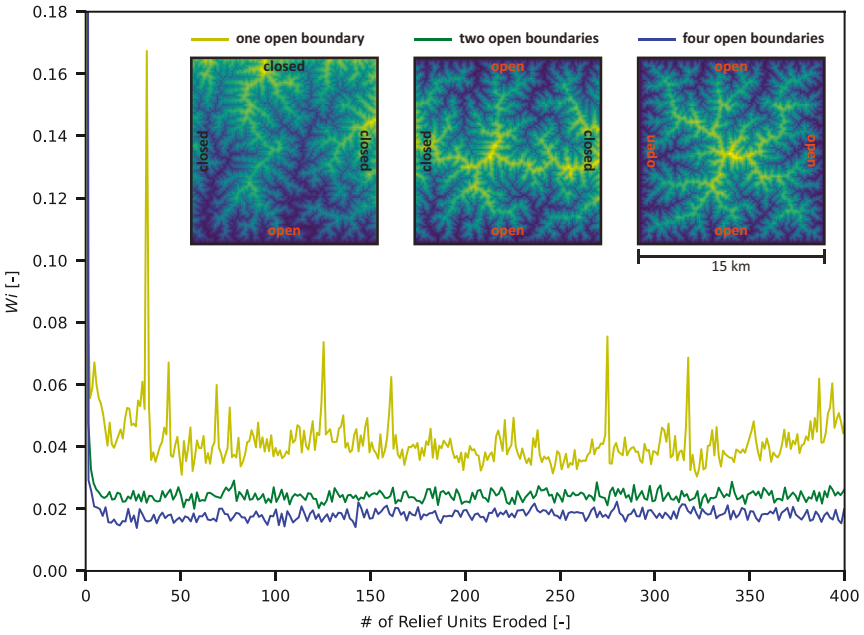

Fig. 4. Time series of wiggle number for three LEM-wLE simulations using different boundary conditions. The wiggle number decreases when the boundary conditions change from closed to open.

dramatic changes in allogenic forcing (37) or spatiotemporal variability in climate (38) and lithology (39) for ridge migration or stream capture to occur. In contrast, LEM-wLE features persistent drainage reorganization that is internally generated (i.e., autogenic) due to lateral channel erosion.

Researchers have argued that drainage networks in their most basic form without topographic, lithologic, and tectonic constraints should tend toward a dendritic form (2). However, even with uniform steady lithology and tectonics, typical LEMs, like LEM-woLE, amplify topographic features (7) that can produce static steady-state, nondendritic drainage networks (Fig. 2*A*). LEM-wLE instead reorganizes the drainage network into a dendritic form, erasing the memory of its initial condition. We note that after eroding through 10 RUs, parts of the sinusoidal channel are still apparent in the LEM-wLE simulation (Fig. 2*B*). Assuming $U = 1$ mm/y, and relief ~= 200 m, this landscape represents 2 My of erosion. We believe it is important to first understand how geomorphic processes behave in the simplest case. However, over this long period, the assumptions that rock type is homogenous and that forcing is steady and uniform become unrealistic. Therefore, a future direction of this work will be to study how drainage networks impacted by complex spatiotemporal variability in tectonics, climate, and lithology reorganize when subjected to lateral erosion.

The rate of initial condition decay and the levels of dynamism in LEM-wLE are dictated by K_L/K_V. Increasing this ratio causes the rate of decay of initial condition signals to accelerate and shifts the equilibrium behavior from a static to a dynamic steady state. Fig. 3 shows that the simulations with higher K_L/K_V values have higher *Wi* values. To understand the extent of the effect of lateral erosion, it is paramount to estimate this ratio. Langston and Tucker (22) hypothesized K_L/K_V to be as follows:

$$\frac{K_L}{K_V} = \frac{k_w\sqrt{R}}{F}, \quad [3]$$

where R is a runoff rate, k_w is a hydraulic geometry constant that relates river width to discharge, and F is a friction factor. Here, the role of lateral erosion becomes more important as runoff (i.e., precipitation) increases. This suggests that climate has an important role in drainage network reorganization, a dependence that is mirrored in landscape experiments (33). In addition. experiments and numerical modeling have shown that sediment can control the pace of bedrock incision (40) and that large blocks can retard river incision (41, 42). Furthermore, lateral channel migration can increase hillslope toe erosion rates that can coarsen sediment grain size distributions (43). In a similar fashion to alluvial river migration (44), it is possible that there is a negative channel–hillslope feedback where large sediment blocks modulate and limit the migration rate in bedrock rivers.

Some flume experiments (28–31) suggest landscapes tend toward a static steady state. However, our results show that open boundary configurations in these experiments (28–31) can suppress dynamism. Open boundary configurations create landscapes dissected by many low-order channels, each containing a relatively small discharge. In contrast, closed configurations promote fewer higher-order channels. In LEM-wLE, a dimensional analysis (45) shows that lateral migration scales with drainage area (*SI Appendix*, Text S1). Therefore, for the same domain size, channels in open configurations migrate less than those in the closed configurations, decreasing the level of dynamism in the landscape. In addition, *SI Appendix*, Fig. S10 shows that for the same boundary configuration, the wiggle number increases with the size of the domain (Movie S31–S39). Our numerical model results potentially resolve the discrepancy between the two divergent experimental results. Last, we note that landscapes with open boundaries can still achieve states with substantial dynamism when the domain, i.e., drainage area, is sufficiently large (see *SI Appendix*, Text S1).

The dynamic steady-state landscapes in LEM-wLE create drainage networks that are in a constant geometric disequilibrium. Willett et al. (9) hypothesize that drainage basin reorganization is driven by landscapes adjusting toward geometric equilibrium. However, topographic analysis of ancient landscapes indicate that geometric equilibrium may be the exception and not the norm (12). Our results suggest that lateral migration of bedrock channels is a plausible mechanism that can cause landscapes to be in a constant state of reorganization, never obtaining a geometric equilibrium. Geometric disequilibrium can also arise from allogenic factors such as spatial heterogeneity in climate, tectonics, and rock properties, or in landscapes in a transient state. Our model, however, implies that geometric disequilibrium can be solely due to autogenic geomorphic processes.

Materials and Methods

LEM-woLE. We utilized a simple LEM based on the stream power incision model (36). The conservation equation can be written as follows:

$$\frac{\partial \eta}{\partial t} = U - K_V A^m S^n, \quad [4]$$

where η is elevation, t is time, U is uplift, K_V is vertical rock erodibility, A is drainage area, m is an exponent, S is slope, and n is an exponent. The second term on the RHS of the equation represents the stream power incision model, which assumes that bedrock erosion scales with drainage area (proxy for river discharge) and downstream slope. We use the following parameters for all the simulations shown: $U = 1$ mm/y; $K_V = 5 \times 10^{-5}$ y^{-1}; $m = 0.5$; and $n = 1.0$ [similarly to Langston and Tucker (22)]. For our simulations, we use a model domain that is 15 × 15 km, a grid size, $dx = 100$ m, and a time step, $dt = 100$ y [maximum Courant (46) number = 0.75]. We use three closed sides (left, right, and top) and one open side (bottom) for our boundary conditions, except where specified. Last, drainage area was computed using an algorithm routes flow over depressions (47).

LEM-wLE. In this study, we use the theory and numerical implementation of Langston and Tucker (22) (see *SI Appendix*, Text S2 for more details) to simulate lateral erosion in bedrock channels. In their formulation, lateral erosion is inversely proportional to the planform radius of curvature, r_c:

$$E_L = \frac{K_L A S}{r_c}, \quad [5]$$

where E_L is lateral erosion and K_L is lateral rock erodibility. In this study, we utilize the total block erosion model, which is appropriate for modeling resistant bedrock (22). The lateral erosion rate is applied to a surface on the banks of the channel. The area of this surface is the product of the bank length and effective flow depth. Flow depth is given as follows:

$$H = k_h Q^{c_h}, \quad [6]$$

where H is depth, Q is flow discharge, and k_h and c_h are positive coefficients. Here, $k_h = 0.4$, $c_h = 0.35$, and H and Q are given (48) in units of meters and cubic meters per second, respectively. Discharge is calculated as follows:

$$Q = RA, \quad [7]$$

where R is a runoff rate. In our simulations, we assume R is a uniform value equal to 100 m/y. This rate represents runoff that drives the dominant discharge that most contributes to channel change. In our model, a term that accounts for the intermittency of this flow is built into the erodibility terms.

It should also be noted that a depositional component is included algorithm of Langston and Tucker (22). For simplification, our analysis assumes that the landscape is completely detachment-limited, so that deposition of material is neglected.

Data and Code Availability. Animations and data of our simulations have been deposited in the Illinois Data Bank (https://databank.illinois.edu/datasets/IDB-1558455) (49). Our code with the associated driver files can be found at GitHub (https://github.com/jeffskwang/LEM-wLE) (50). The lateral incision submodel of Langston and Tucker (22) can also be found in the Python toolkit, LANDLAB (https://landlab.github.io/#) (51, 52).

ACKNOWLEDGMENTS. J.S.K. acknowledges funding from the NSF Graduate Research Fellowship Program through Grant DGE-1144245. J.S.K. and G.P. acknowledge funding from the NSF through Grant EAR-1427262. A.L.L. acknowledges funding from the NSF through Grant OIA-1833025.

1. E. R. Zernitz, Drainage patterns and their significance. *J. Geol.* **40**, 498–521 (1932).
2. A. I. Mejía, J. D. Niemann, Identification and characterization of dendritic, parallel, pinnate, rectangular, and trellis networks based on deviations from planform self-similarity. *J. Geophys. Res.* **113**, F02015 (2008).
3. I. Rodríguez-Iturbe *et al*., Energy dissipation, runoff production, and the three-dimensional structure of river basins. *Water Resour. Res.* **28**, 1095–1103 (1992).
4. A. Rinaldo, R. Rigon, J. R. Banavar, A. Maritan, I. Rodriguez-Iturbe, Evolution and selection of river networks: Statics, dynamics, and complexity. *Proc. Natl. Acad. Sci. U.S.A.* **111**, 2417–2424 (2014).
5. A. Tejedor, A. Singh, I. Zaliapin, A. L. Densmore, E. Foufoula-Georgiou, Scale-dependent erosional patterns in steady-state and transient-state landscapes. *Sci. Adv.* **3**, e1701683 (2017).
6. J. T. Hack, Interpretation of erosional topography in humid temperate regions. *Am. J. Sci.* **258-A**, 80–97 (1960).
7. J. S. Kwang, G. Parker, Extreme memory of initial conditions in numerical landscape evolution models. *Geophys. Res. Lett.* **46**, 6563–6573 (2019).
8. S. D. Willett, R. Slingerland, N. Hovius, Uplift, shortening, and steady state topography in active mountain belts. *Am. J. Sci.* **301**, 455–485 (2001).
9. S. D. Willett, S. W. McCoy, J. T. Perron, L. Goren, C.-Y. Chen, Dynamic reorganization of river basins. *Science* **343**, 1248765 (2014).
10. J. T. Perron, L. Royden, An integral approach to bedrock river profile analysis. *Earth Surf. Process. Landf.* **38**, 570–576 (2013).
11. L. E. Hasbargen, C. Paola, Landscape instability in an experimental drainage basin. *Geology* **28**, 1067 (2000).
12. H. W. Beeson, S. W. McCoy, A. Keen-Zebert, Geometric disequilibrium of river basins produces long-lived transient landscapes. *Earth Planet. Sci. Lett.* **475**, 34–43 (2017).
13. J. T. Perron, S. Fagherazzi, The legacy of initial conditions in landscape evolution. *Earth Surf. Process. Landf.* **37**, 52–63 (2012).
14. A. D. Howard, Theoretical model of optimal drainage networks. *Water Resour. Res.* **26**, 2107–2117 (1990).
15. K. N. Johnson, N. J. Finnegan, A lithologic control on active meandering in bedrock channels. *Geol. Soc. Am. Bull.* **127**, 1766–1776 (2015).
16. T. Inoue, G. Parker, C. P. Stark, Morphodynamics of a bedrock-alluvial meander bend that incises as it migrates outward: Approximate solution of permanent form: Morphodynamics of a bedrock-alluvial meander bend. *Earth Surf. Process. Landf.* **42**, 1342–1354 (2017).
17. N. J. Finnegan, W. E. Dietrich, Episodic bedrock strath terrace formation due to meander migration and cutoff. *Geology* **39**, 143–146 (2011).
18. G. S. Hancock, R. S. Anderson, Numerical modeling of fluvial strath-terrace formation in response to oscillating climate. *Geol. Soc. Am. Bull.* **114**, 1131–1142 (2002).
19. G. Y. Brocard, P. A. van der Beek, "Influence of incision rate, rock strength, and bedload supply on bedrock river gradients and valley-flat widths: Field-based evidence and calibrations from western Alpine rivers (southeast France)" in *Tectonics, Climate, and Landscape Evolution*, S. D. Willett, N. Hovius, M. T. Brandon, D. M. Fisher, Eds. (Geological Society of America, 2006), pp. 101–126.
20. A. L. Langston, A. J. A. M. Temme, Bedrock erosion and changes in bed sediment lithology in response to an extreme flood event: The 2013 Colorado Front Range flood. *Geomorphology* **328**, 1–14 (2019).
21. G. K. Gilbert, *Geology of the Henry Mountains* (Government Printing Office, 1877).
22. A. L. Langston, G. E. Tucker, Developing and exploring a theory for the lateral erosion of bedrock channels for use in landscape evolution models. *Earth Surf. Dyn.* **6**, 1–27 (2018).
23. D. J. Jerolmack, C. Paola, Shredding of environmental signals by sediment transport. *Geophys. Res. Lett.* **37**, L19401 (2010).
24. S. D. Willett, M. T. Brandon, On steady states in mountain belts. *Geology* **30**, 175 (2002).
25. J. D. Pelletier, Persistent drainage migration in a numerical landscape evolution model. *Geophys. Res. Lett.* **31**, L20501 (2004).
26. J. T. Perron, W. E. Dietrich, J. W. Kirchner, Controls on the spacing of first-order valleys. *J. Geophys. Res.* **113**, F04016 (2008).
27. A. L. Densmore, M. A. Ellis, R. S. Anderson, Landsliding and the evolution of normal-fault-bounded mountains. *J. Geophys. Res. Solid Earth* **103**, 15203–15219 (1998).
28. S. Bonnet, A. Crave, Landscape response to climate change: Insights from experimental modeling and implications for tectonic versus climatic uplift of topography. *Geology* **31**, 123 (2003).
29. D. Lague, A. Crave, P. Davy, Laboratory experiments simulating the geomorphic response to tectonic uplift. *J. Geophys. Res. Solid Earth* **108**, ETG 3-1–ETG 3-20 (2003).
30. J. Babault, S. Bonnet, A. Crave, J. Van Den Driessche, Influence of piedmont sedimentation on erosion dynamics of an uplifting landscape: An experimental approach. *Geology* **33**, 301 (2005).
31. S. Bonnet, A. Crave, Macroscale dynamics of experimental landscapes. *Geol. Soc. Lond. Spec. Publ.* **253**, 327–339 (2006).
32. L. Reinhardt, M. A. Ellis, The emergence of topographic steady state in a perpetually dynamic self-organized critical landscape. *Water Resour. Res.* **51**, 4986–5003 (2015).
33. A. Singh, L. Reinhardt, E. Foufoula-Georgiou, Landscape reorganization under changing climatic forcing: Results from an experimental landscape. *Water Resour. Res.* **51**, 4320–4337 (2015).
34. K. E. Sweeney, J. J. Roering, C. Ellis, GEOMORPHOLOGY. Experimental evidence for hillslope control of landscape scale. *Science* **349**, 51–53 (2015).
35. C. Paola, K. Straub, D. Mohrig, L. Reinhardt, The "unreasonable effectiveness" of stratigraphic and geomorphic experiments. *Earth Sci. Rev.* **97**, 1–43 (2009).
36. A. D. Howard, A detachment-limited model of drainage basin evolution. *Water Resour. Res.* **30**, 2261–2285 (1994).
37. K. X. Whipple, A. M. Forte, R. A. DiBiase, N. M. Gasparini, W. B. Ouimet, Timescales of landscape response to divide migration and drainage capture: Implications for the role of divide mobility in landscape evolution: Landscape response to divide mobility. *J. Geophys. Res. Earth Surf.* **122**, 248–273 (2017).
38. A. M. Anders, G. H. Roe, D. R. Montgomery, B. Hallet, Influence of precipitation phase on the form of mountain ranges. *Geology* **36**, 479 (2008).
39. S. F. Gallen, Lithologic controls on landscape dynamics and aquatic species evolution in post-orogenic mountains. *Earth Planet. Sci. Lett.* **493**, 150–160 (2018).
40. L. S. Sklar, W. E. Dietrich, Sediment and rock strength controls on river incision into bedrock. *Geology* **29**, 1087–1090 (2001).
41. C. M. Shobe, G. E. Tucker, R. S. Anderson, Hillslope-derived blocks retard river incision. *Geophys. Res. Lett.* **43**, 5070–5078 (2016).
42. R. C. Glade, C. M. Shobe, R. S. Anderson, G. E. Tucker, Canyon shape and erosion dynamics governed by channel-hillslope feedbacks. *Geology* **47**, 650–654 (2019).
43. L. S. Sklar *et al*., The problem of predicting the size distribution of sediment supplied by hillslopes to rivers. *Geomorphology* **277**, 31–49 (2017).
44. G. Parker *et al*., A new framework for modeling the migration of meandering rivers. *Earth Surf. Process. Landf.* **36**, 70–86 (2011).
45. N. Theodoratos, H. Seybold, J. W. Kirchner, Scaling and similarity of a stream-power incision and linear diffusion landscape evolution model. *Earth Surf. Dyn.* **6**, 779–808 (2018).
46. R. Courant, H. Lewy, K. Friedrichs, Über die partiellen Differenzengleichungen der mathematischen Physik. *Math. Ann.* **100**, 32–74 (1928).
47. O. Planchon, F. Darboux, A fast, simple and versatile algorithm to fill the depressions of digital elevation models. *Catena* **46**, 159–176 (2002).
48. E. D. Andrews, Bed-material entrainment and hydraulic geometry of gravel-bed rivers in Colorado. *Bull. Geol. Soc. Am.* **95**, 371–378 (1984).
49. J. S. Kwang, A. L. Langston, G. Parker, Dataset for "The necessity of lateral channel migration in the evolution of non-dendritic drainage networks to full dendricity and the persistence of dynamic networks." Illinois Data Bank. https://databank.illinois.edu/datasets/IDB-1558455. Deposited 27 January 2021.
50. J. S. Kwang, jeffskwang/LEM-wLE: LEM-wLE_v1.0. GitHub. https://github.com/jeffskwang/LEM-wLE. Deposited 18 October 2020.
51. D. E. J. Hobley *et al*., Creative computing with Landlab: an open-source toolkit for building, coupling, and exploring two-dimensional numerical models of Earth-surface dynamics. *Earth Surf. Dyn.* **5**, 21–46 (2017).
52. K. R. Barnhart *et al*., Short communication: Landlab v2.0: a software package for Earth surface dynamics. *Earth Surf. Dynam.* **8**, 379–397 (2020).
53. R. E. Horton, Drainage-basin characteristics. *Eos (Wash. D.C.)* **13**, 350–361 (1932).
54. R. E. Horton, Erosional development of streams and their drainage basins; hydrophysical approach to quantitative morphology. *Bull. Geol. Soc. Am.* **56**, 275–370 (1945).
55. A. N. Strahler, Hypsometric (area-altitude) analysis of erosion topography. *Bull. Geol. Soc. Am.* **63**, 1117–1142 (1952).
56. A. N. Strahler, Quantitative analysis of watershed geomorphology. *Eos (Wash. D.C.)* **38**, 913–920 (1957).